ϵ-Shell error analysis for "Walk On Spheres" algorithms

Michael Mascagni [a], Chi-Ok Hwang [b],[*],[1]

[a] *Department of Computer Science, Florida State University, 203 Love Building Tallahassee, FL 32306-4530, USA*
[b] *Innovative Technology Center for Radiation Safety, Hanyang University, HIT Building, 17 Haengdang-Dong, Sungdong-Gu, Seoul 133-791, South Korea*

Abstract

The "Walk On Spheres" (WOS) algorithm and its relatives have long been used to solve a wide variety of boundary value problems [Ann. Math. Stat. 27 (1956) 569; J. Heat Transfer 89 (1967) 121; J. Chem. Phys. 100 (1994) 3821; J. Appl. Phys. 71 (1992) 2727]. All WOS algorithms that require the construction of random walks that terminate, employ an ϵ-shell to ensure their termination in a finite number of steps. To remove the error related to this ϵ-shell, Green's function first-passage (GFFP) algorithms have been proposed [J. Chem. Phys. 106 (1997) 3721] and used in several applications [Phys. Fluids A 12 (2000) 1699; Monte Carlo Meth. Appl. 7 (2001) 213; The simulation–tabulation method for classical diffusion Monte Carlo, J. Comput. Phys. submitted]. One way to think of the GFFP algorithm is as an $\epsilon = 0$ extension of WOS. Thus, an important open question in the use of GFFP is to understand the tradeoff made in the efficiency of GFFP versus the ϵ-dependent error in WOS. In this paper, we present empirical evidence and analytic analysis of the ϵ-shell error in some simple boundary value problems for the Laplace and Poisson equations and show that the error associated with the ϵ-shell is O(ϵ), for small ϵ. This fact supports the conclusion that GFFP is preferable to WOS in cases where both are applicable.
© 2003 IMACS. Published by Elsevier Science B.V. All rights reserved.

PACS: 87.15.Vv; 84.37.+q; 82.20.Pm

Keywords: Walk On Spheres (WOS); Error; Laplace; Poisson

1. Introduction

In general, Monte Carlo random walk algorithms inside a domain [5] can be classified into two broad categories: random walks on grids or other discrete objects [6] and continuous, grid-free, random walks/Brownian motions. Among these Monte Carlo algorithms, the grid-free "Walk On Spheres"

* Corresponding author. Tel.: +82-2-22918154; fax: +82-2-22968154.
E-mail address: chwang@itrs.hanyang.ac.kr (C.-O. Hwang).

[1] Present address: Computational Electronics Center, Inha University, 253 Yonghyeon-dong, Nam-gu, Incheon 402-751, South Korea.

(WOS) algorithm is among the most popular. In WOS, one does not simulate details of the Wiener process inside the domain, instead discrete jumps are made using the uniform first-passage probability distribution of Brownian motion from the center to the surface of a sphere.

WOS algorithms have been used to solve Dirichlet problems for a wide variety of both elliptic and parabolic partial differential equations (PDEs). The first such description of the use of WOS for PDEs was when Müller applied WOS to solve the Dirichlet problem for the Laplace equation [1]. Later Haji-Sheikh and Sparrow developed the WOS method for the Poisson equation with a nonzero but constant source term [2]. The related equation $\Delta u - cu = -g$ was solved by Elepov and Mikhailov [7] using a modified WOS method, and Booth used a weighted WOS method to solve homogeneous elliptic PDEs with constant coefficients [8,9].

All the above methods involving WOS employ an ϵ-shell to terminate the random walks. The boundary, which random walks terminate on, is thickened by ϵ, and when a walker enters this ϵ-shell, the walk is terminated by choosing a boundary point closest to this point in the ϵ-shell (usually the point in the ϵ-shell is normal from the chosen boundary point). The use of this ϵ-shell entails an error; however, this ϵ-shell error can, in general, always be made smaller than the statistical sampling error [9,8]. A technique for empirically estimating this ϵ-shell error uses a single random walk to both estimate the ϵ and the $\epsilon/10$ error. The difference between these two correlated estimates gives a measure of the ϵ behavior of the error due to the finite width of the ϵ-shell. By adjusting ϵ, one can make this error less than that arising from the statistical sampling error. Thus, if one increases the number of random walks in order to decrease the statistical error, one must also reduce ϵ to reduce the ϵ-shell error to balance the two errors. However, reducing ϵ also increases the running time as the average number of steps required for a random walk to be absorbed in the ϵ-shell in WOS is O($|\ln \epsilon|$) [5].

Recently, a technique for removing the need for the ϵ-shell for certain geometries was developed by using a set of Green's functions to provide exact first-passage probability distributions to terminate the walks [4]. The ϵ-shell was removed by allowing spherical first-passage surfaces to intersect the target surface. On the geometry defined by these intersecting surfaces, exact first-passage probability distributions were used to exactly terminate the walks. For a given geometry, the boundary Green's function is exactly equal to the first-passage probability distribution of Brownian motion, and so by precomputing the appropriate Green's functions, exact first-passage probability distributions can be used. Using these first-passage distributions in WOS to terminate the walks exactly and without the need of the ϵ-shell is called the Green's function first-passage (GFFP) algorithm [4]. Since its inception, the GFFP algorithm has been extended and refined to allow it to be applied to a wide variety of problems and applications [10,11].

The O(ϵ) error due to the WOS ϵ-shell was a phenomenon that was both well known and poorly studied. Thus, we feel it timely to publish a study that analyzes the ϵ-shell error. We provide a more rigorous basis for the O(ϵ) error result to support the efficiency of GFFP versus WOS when accuracy beyond a preset limit is required [11]. In general, it has been assumed that the accuracy attainable in a simulation in WOS is O($\epsilon^{1/\gamma}$) for small ϵ for some $\gamma > 0$ [12]. But very little data is available to quantify this. In this paper, we investigate the ϵ-shell error, determine the value of γ in the case where we have a smooth boundary and analyze this error.

This paper is organized as follows: in Section 2, we investigate the ϵ-shell error by simulating WOS solutions of some simple Dirichlet boundary value problems (BVPs) for both the Laplace and Poisson equations. In Section 3, we give an analytic analysis of the simulation results of the ϵ-shell error and provide some concluding remarks.

2. ϵ-Error analysis

In this section, we empirically analyze the ϵ-shell error for WOS with several examples. This error associated with ϵ is linear in ϵ in all the cases of Dirichlet BVPs studied. This linearity can also be explained analytically, and can be understood from the point of view of regularity of solutions with respect to boundary values. Given sufficiently smooth boundaries, it is expected that $O(\epsilon)$ perturbations of boundary values will result in $O(\epsilon)$ changes in solution values [13]. Thus, our results are consistent with these intuitive notions.

The errors associated with WOS methods are two-fold. One error originates from the algorithm's Monte Carlo nature and the second error from the ϵ-shell. The first error is a purely statistical error associated with the uncertainty in estimating a mean from N samples. This error is $O(N^{1/2})$, and is measured by invoking the law of large numbers and assuming the sum of N mean samples is approximately normally distributed. This error can be reduced by increasing the number of random samples, which in the WOS case means increasing the number of random walks. The other error we wish to study is the error from the ϵ-shell. To do so empirically one must make sure that the sampling error is made much smaller than the ϵ-shell error to expose it to empirical scrutiny. Thus, in this study we always choose N sufficiently large so that the error from statistical sampling is much less than that expected from the ϵ-shell. In fact, the N used in this study will be considerably larger than that usually required in solving BVPs with WOS, since we wish to completely expose the ϵ-shell error. It is important to remember that for problems solvable with the GFFP method, the ϵ-shell error is zero.

We now consider the numerical solution of several Dirichlet BVPs for both the Laplace and Poisson equations. The exact problems solved range from extremely simple to somewhat complicated yet idealized problems for which analytic solutions are known. We consider Dirichlet BVPs for the Laplace equation with a constant boundary function, the Laplace equation with a non-constant boundary function, and the Poisson equation.

2.1. The Laplace equation with constant boundary functions

In this section, we will consider solving several Dirichlet BVPs with constant boundary functions for the Laplace equations. These problems come from rather concrete applications which include computing the capacitance of a unit sphere, solving the ligand-protein caricature Solc-Stockmayer model without potential, and computing the mean survival time in a composite material made up of a uniform matrix with inclusions of nonoverlapping spherical traps.

2.1.1. The capacitance of a sphere

The electrostatic capacitance of an arbitrarily shaped conducting object can be calculated by adapting the algorithm originally devised for calculating the diffusion-controlled reaction rate toward the target object as follows [3]. The capacitance, C, of an arbitrarily shaped conducting object can be obtained by computing the probability, β, of Brownian motion started on a sphere of radius b completely enclosing the given object, and doing first passage on the object:

$$C = b\beta. \tag{1}$$

Here, b is the radius of the "launching sphere," containing the given object, where Brownian walkers are started, and β is computed by counting the frequency of walkers that do first passage on the given object instead of walking to infinity without striking the object.

This electrostatic capacitance problem is a Dirichlet BVP for the Laplace equation in the following sense. Let $\phi(x)$ be the electrostatic potential satisfying the following Laplace equation:

$$\Delta\phi(x) = 0, \quad x \in \Omega, \tag{2}$$

with the boundary conditions,

$$\phi(x) = 1, \quad x \in \partial\Omega, \tag{3}$$

$$\phi(x) = 0, \quad as \quad x \to \infty. \tag{4}$$

The capacitance of a conductor is the total charge on the conductor at unit potential [14]. Thus, the capacitance of the conductor is given by:

$$C = -(4\pi)^{-1} \int_{\partial\Omega} d\sigma \cdot \nabla\phi(x) = (4\pi)^{-1} \int_{\partial\Omega} d\sigma \cdot \nabla p(x). \tag{5}$$

Here, the relationship between the electrostatic potential, $\phi(x)$, and the probability density of Brownian walkers, $p(x)$, is given by $\phi(x) = 1 - p(x)$. The diffusion-controlled reaction rate, κ, toward the target object is [3]

$$\kappa = D \int_{\partial\Omega} d\sigma \cdot \nabla p(x) = \kappa(b)\beta = 4\pi Db\beta, \tag{6}$$

where $\kappa(b)$ is the diffusion-controlled reaction rate of the launching sphere of radius b and D is the diffusion coefficient. From the above two equations, we obtain Eq. (1).

The simplest problem of this type is to calculate the capacitance of a unit sphere, which is known to be equal to one (see Fig. 1). This computation reduces to computing the probability of a Brownian particle started on a large sphere containing the unit sphere and doing first-passage on the unit sphere instead of walking to infinity. Here, we compute this value using WOS with $N = 10^8$ random walks. The results are
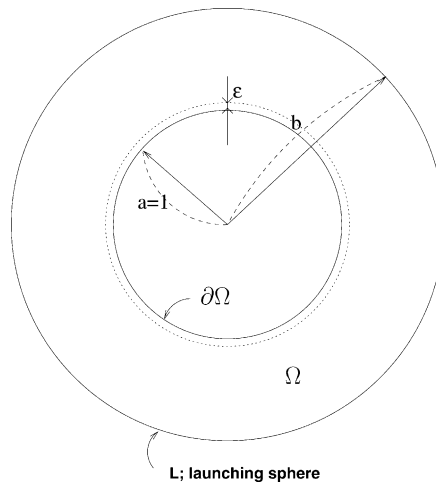

Fig. 1. A schematic diagram that illustrates the calculation of the capacitance of a unit sphere; L is the launching sphere with radius b where Brownian particles are initiated with uniform probability distribution.
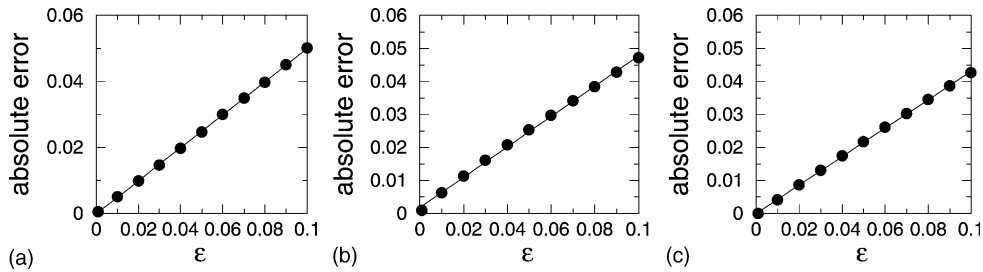
Fig. 2. Computed ϵ-related errors for the solution to three elliptic BVPs with constant boundary values. Solid lines show linear regression results. The errors are linear in ϵ. In the separate panels, we plot absolute errors versus ϵ for the following cases: (a) the electrostatic capacitance of a unit conducting sphere, (b) the reaction rate constant $\kappa/4\pi Da$ for the Solc-Stockmayer model without potential, and (c) the average survival time for nonoverlapping impenetrable spheres.

plotted in Fig. 2a. With the ϵ-shell, we terminate random walks when they are within ϵ of the boundary. As we see from the figure, the absolute error is linear in ϵ. The computed capacitance of the unit sphere we obtain with an ϵ-shell can be interpreted by assuming that we are actually computing the capacitance of a sphere with an average radius of $1 + \epsilon/2$.

2.1.2. Solc-Stockmayer model without potential

We next consider the Solc-Stockmayer model without potential, a basic model for computing the reaction rate of diffusion-limited protein-ligand binding. A protein molecule is modeled as a sphere with a circular patch on its surface producing irreversible binding upon contact with a diffusing ligand. The ligand undergoes Brownian motion and we measure the probability of the ligand hitting the reactive patch or diffusing to infinity. Ligand molecules are idealized as non-interacting point-like diffusing particles. Moreover, the portion of the sphere not covered by the reacting patch is considered to have a reflecting boundary with respect to the Brownian ligand particle. This reaction rate problem is clearly analogous to the Dirichlet BVP arising in the electrostatic capacitance problem of a unit sphere except that this problem has a reflecting boundary condition on the non-reactive portion of the sphere.

The basic method used here for the calculation of the reaction rate is the capture probability method [15] (see Fig. 3). We simulate diffusing ligands that begin on a "launch sphere" of radius b, surrounding the target sphere, i.e. the protein model. Each diffusing ligand starts its random walk on the launch sphere at a position chosen at random (see Fig. 3). The ligand then makes first-passage jumps until it either reaches the reactive patch on the target sphere, or diffuses to infinity. The reaction rate constant, κ, is given by [16]

$$\frac{\kappa}{4\pi Da} = b\beta, \tag{7}$$

where b is the launching sphere radius and a the target sphere radius, β the fraction of diffusing ligands from the launching sphere that are absorbed on the reactive patch, and D the diffusion coefficient.

To study the ϵ-dependent errors, the exact values are obtained by the method of dual series relations [17]. Fig. 2b shows the absolute error of this Solc-Stockmayer reaction rate computation averaging $N = 10^8$ diffusing ligand trajectories and using a circular reactive patch subtending a solid angle of $\Theta = 20°$. The figure shows that once again the ϵ error is linear in ϵ.
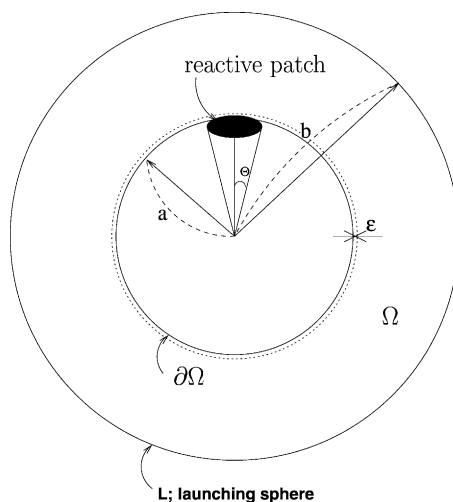
Fig. 3. A schematic diagram that illustrates the simple Solc-Stockmayer model for diffusion-limited protein-ligand binding. *L* is the launching sphere with radius *b* where a diffusing ligand is launched with uniform probability distribution, and *Ω* is a protein of radius $a = 1.0$ with a circular reactive patch with angle *Θ*. The reactive patch is absorbing and the rest of the protein reflecting.

2.1.3. Average survival time in nonoverlapping spherical traps

Next we compute the mean survival time of noninteracting Brownian particles diffusing in a volume containing nonoverlapping spherical traps. This problem is an example of a composite medium computation. For the mathematical formulation, let us start with the Feyman–Kac path-integral representation for solving the Dirichlet problem for Poisson's equation:

$$\Delta u(\boldsymbol{x}) = q(\boldsymbol{x}), \quad \boldsymbol{x} \in \Omega, \tag{8}$$

$$u(\boldsymbol{x}) = 0, \quad \boldsymbol{x} \in \partial\Omega. \tag{9}$$

The solution to this problem, given in the form of the path-integral with respect to standard Brownian motion $X_t^{\boldsymbol{x}}$, is as follows [18,19]:

$$u(\boldsymbol{x}) = E\left[-\int_0^{\tau^{\boldsymbol{x}}} q(X_t^{\boldsymbol{x}}) \, \mathrm{d}t\right]. \tag{10}$$

Here, $\tau^{\boldsymbol{x}}$ is the first-passage time of a Brownian particle starting at $\boldsymbol{x}$. We can see that when $q(\cdot) = -1$, $u(\boldsymbol{x}) = E[\int_0^{\tau^{\boldsymbol{x}}} \mathrm{d}t] = E[\tau^{\boldsymbol{x}}]$. Thus, computing the mean fist-passage time (survival time) is also a Dirichlet boundary problem for the Poisson equation with a constant source [20]:

$$\Delta u(\boldsymbol{x}) = -1, \quad \boldsymbol{x} \in \Omega, \tag{11}$$

and with the homogeneous boundary conditions

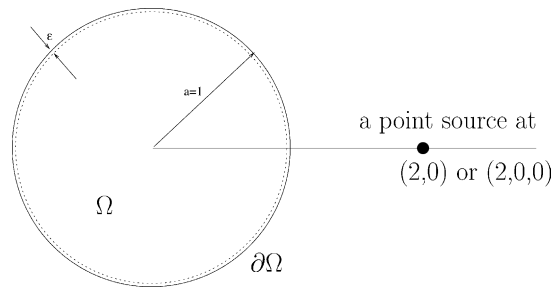$$u(\boldsymbol{x}) = 0, \quad \boldsymbol{x} \in \partial\Omega. \tag{12}$$

Fig. 4. A schematic diagram that illustrates the geometry for a simple Laplace problem with a point source outside of the circular (or spherical) boundary.

In our example the mean survival time was computed in a medium that consists of 572 nonoverlapping spheres with radius $a = 1.0$, and has a sink volume fraction[2] of $\phi_2 = 0.3$ using $N = 10^8$ random walks. The absolute error in this computation with the WOS method again shows linearity in ϵ as seen in Fig. 2c. The expected exact value was obtained through a linear regression of the simulation data points.

2.2. Simple Laplace problems with non-constant Dirichlet boundary conditions

Next, we consider the Dirichlet problem for the Laplace equation in the two-dimensional unit circle, Ω (see Fig. 4):

$$\Delta u(\boldsymbol{x}) = 0, \quad \boldsymbol{x} \in \Omega, \tag{13}$$

with the boundary condition,

$$u(\boldsymbol{x}) = \tfrac{1}{2} \ln[(x_1 - 2)^2 + x_2^2], \quad \text{for} \quad |\boldsymbol{x}| = 1 \quad (\boldsymbol{x} \in \partial\Omega). \tag{14}$$

We write $\boldsymbol{x} = (x_1, x_2)$, and can compute that the exact solution is given by

$$u(\boldsymbol{x}) = \tfrac{1}{2} \ln[(x_1 - 2)^2 + x_2^2], \quad \boldsymbol{x} \in \Omega. \tag{15}$$

The boundary conditions for this problem are consistent with placing a point source at $(2, 0)$ and computing the potential imposed on the boundary of the unit circle. We then evaluated the ϵ-shell errors at the single point $(0.2, -0.5) \in \Omega$ again using $N = 10^8$ random walks.

We next consider the Dirichlet problem for the Laplace equation in the three-dimensional unit sphere, Ω (see Fig. 4):

$$\Delta u(\boldsymbol{x}) = 0, \quad \boldsymbol{x} \in \Omega, \tag{16}$$

with boundary condition

$$u(\boldsymbol{x}) = [(x_1 - 2)^2 + x_2^2 + x_3^2]^{-1/2}, \quad \text{for} \quad |\boldsymbol{x}| = 1. \tag{17}$$

Again we write $\boldsymbol{x} = (x_1, x_2, x_3)$, and have the exact solution given as

$$u(\boldsymbol{x}) = [(x_1 - 2)^2 + x_2^2 + x_3^2]^{-1/2}, \quad \boldsymbol{x} \in \Omega. \tag{18}$$

---

[2] The sink volume fraction is the fraction of the whole volume occupied by the nonoverlapping spheres. This concept is identical to that of the porosity of a porous medium.
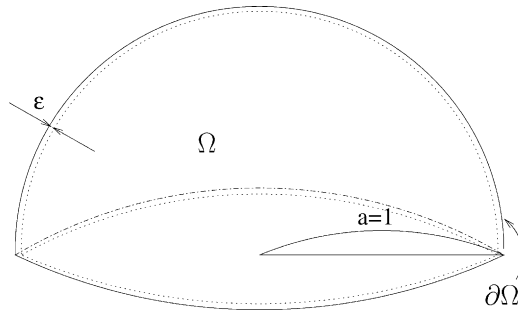
Fig. 5. A schematic diagram that illustrates the geometry for a simple Laplace problem with boundary conditions on a hemisphere.

This solution is derived by placing a point source at (2, 0, 0) for the free-space Laplace equation and computing the induced boundary condition on the surface of the unit sphere. In this study we analyze the errors at the point $(0.2, 0.3, -0.1)$ by using $N = 10^9$ random walks.

Finally, we consider the Dirichlet problem for the Laplace equation in a hemisphere, Ω, with geometry as depicted in Fig. 5 [5]. Again we solve the Laplace equation:

$$\Delta u(\boldsymbol{x}) = 0, \quad \boldsymbol{x} \in \Omega, \tag{19}$$

with the particular boundary conditions

$$u(\boldsymbol{x}) = [2(x_3 + 1)]^{-1/2}, \quad \text{for} \quad |\boldsymbol{x}| = 1, \tag{20}$$

and

$$u(\boldsymbol{x}) = [(x_1^2 + x_2^2 + 1)]^{-1/2}, \quad \text{for} \quad x_3 = 0. \tag{21}$$

The exact solution is known to be

$$u(\boldsymbol{x}) = [(x_1^2 + x_2^2 + (x_3 + 1)^2)]^{-1/2}, \quad \boldsymbol{x} \in \Omega. \tag{22}$$

Here, we analyze the errors associated with the ϵ-shell at the point$(0.2, 0.3, 0.1)$ with 10^9 random walks. All the absolute error results in Fig. 6 again show the linearity in ϵ.
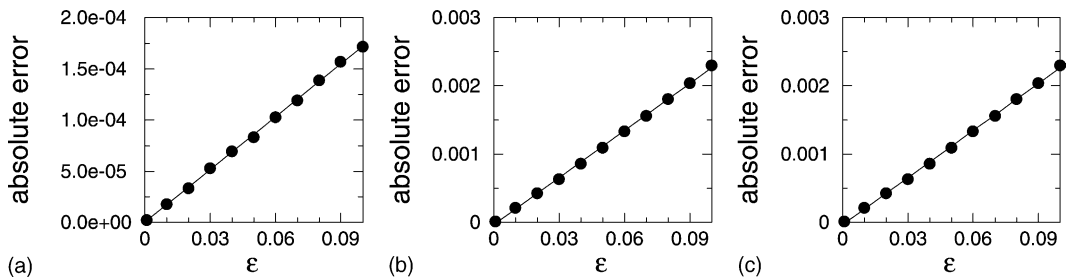

Fig. 6. Computed ϵ-related errors for the solution to three elliptic BVPs with non-constant boundary values. Solid lines show linear regression results supporting the view that the ϵ errors are linear in ϵ. In the separate panels, we plot absolute errors versus ϵ for the following cases: (a) a 2D Laplace problem, (b) a 3D Laplace problem, and (c) a 3D hemisphere Laplace problem.
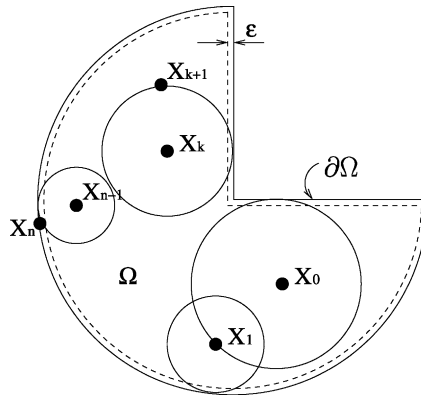
Fig. 7. Modified WOS for the Poisson problem: $X_0, X_1, \ldots, X_k, \ldots, X_n$ are a series of discrete propagation jumps of a Brownian path that terminates with first passage upon Ω. ϵ is the ϵ-shell thickness.

2.3. The Poisson equation

Here, we consider the following particular Dirichlet problem for the Poisson equation

$$\Delta u(\boldsymbol{x}) = -(2 - r^2)\mathrm{e}^{-r^2/2}, \quad \boldsymbol{x} \in \Omega, \tag{23}$$

in a domain, Ω, composed of the unit disk minus the first quadrant. This is the same problem as that used in previous Monte Carlo work on solving the Poisson equation [12]. For a picture of this domain, refer to Fig. 7:

$$\Omega = \{(r, \theta) : 0 < r < 1, -3\pi/2 < \theta < 0\}. \tag{24}$$

The boundary conditions we impose are the following: on the straight parts of the boundary, $u(r, 0) = \mathrm{e}^{-r^2/2}$, $u(r, -3\pi/2) = -r^{1/3} + \mathrm{e}^{-r^2/2}$, and $u(1, \theta) = \sin(\theta/3) + \mathrm{e}^{-1/2}$ on the curved part of the boundary. The analytic solution is known to be

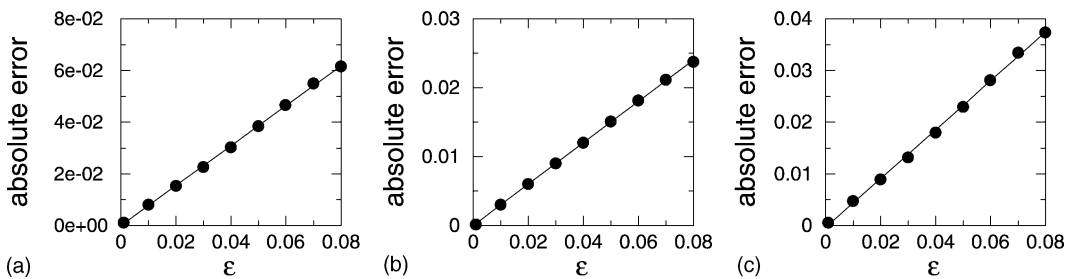$$u(r, \theta) = r^{1/3} \sin(\theta/3) + \mathrm{e}^{-r^2/2}. \tag{25}$$

Fig. 8. Computed ϵ-related errors for the solution to the Poisson equation. Solid lines show linear regression results. The errors are linear in ϵ. In the separate panels, we plot absolute errors versus ϵ for the following cases: (a) the Laplace term of the Poisson problem, (b) the Poisson term of the Poisson problem, and (c) total errors in the Poisson problem.

We evaluate the ϵ-shell errors at the point $(r, \theta) = (0.1244, -0.7906)$ with $N = 10^9$ random walks. In Fig. 8a, the absolute errors from the Laplace term (the error associated with the mean value of the exit points of random walks, see Section 3 for the definition of this term) are shown, in Fig. 8b, the absolute errors from the Poisson term (the error associated with the source term in the Poisson equation, see Section 3 for the definition of this term) and in Fig. 8c, we show the total absolute errors. All display the expected linearity in ϵ.

3. Discussions and conclusions

In this section, we analyze the simulation results of the ϵ-shell error and discuss the WOS method. All problems solved in this paper are mathematically of the following form:

$$\Delta u(\boldsymbol{x}) = q(x), \quad \boldsymbol{x} \in \Omega, \tag{26}$$

with a boundary condition

$$u_0(\boldsymbol{x}) = f(x), \quad \boldsymbol{x} \in \partial\Omega. \tag{27}$$

The integral representation for the solution to this Dirichlet problem for the Poisson equation is given by

$$u(\boldsymbol{x}) = -\int_{\partial\Omega} g(\boldsymbol{x}, \boldsymbol{y}) u_0(\boldsymbol{y}) \, \mathrm{d}\sigma + \int_{\Omega} G(\boldsymbol{x}, \boldsymbol{y}) q(\boldsymbol{x}) \, \mathrm{d}y, \quad \boldsymbol{x} \in \Omega. \tag{28}$$

Here, $G(\boldsymbol{x}, \boldsymbol{y})$ is the Green's function defined by

$$\Delta G(\boldsymbol{x}, \boldsymbol{y}) = \delta(\boldsymbol{x} - \boldsymbol{y}), \quad \boldsymbol{x}, \boldsymbol{y} \in \Omega, \tag{29}$$

$$G(\boldsymbol{x}, \boldsymbol{y}) = 0, \quad \boldsymbol{y} \in \Omega. \tag{30}$$

and

$$g(\boldsymbol{x}, \boldsymbol{y}) = \frac{\partial G(\boldsymbol{x}, \boldsymbol{y})}{\partial \boldsymbol{n}_y}, \tag{31}$$

is the surface Green's function, where $\boldsymbol{n}_y$ is the normal unit vector to the absorbing surface, $\partial\Omega$, at $\boldsymbol{y}$. In Eq. (28), we refer to the first term in this integral representation as the Laplace term and the second as the Poisson term.

By introducing an ϵ-shell, we actually use a slightly perturbed (surface) Green's function instead of the actual (surface) Green's function. This is because adding the ϵ-shell actually distorts $\partial\Omega$ by an O(ϵ) amount. This assumption can be partially supported by the fact that in the calculation of the capacitance of a unit sphere the ϵ-shell caused the unit sphere to seem as it is a sphere of radius $1 + \epsilon/2$. The Laplace term error, L_{error} is thus given by

$$L_{\mathrm{error}} = -\int_{\partial\Omega} g(\boldsymbol{x}, \boldsymbol{y} + k\epsilon\boldsymbol{n}_y) \, \mathrm{d}y + \int_{\Omega} g(\boldsymbol{x}, \boldsymbol{y}) \, \mathrm{d}y. \tag{32}$$

while the Poisson term error, P_{error} can be written as

$$P_{\mathrm{error}} = \int_{\Omega} G(\boldsymbol{x}, \boldsymbol{y} + k\epsilon\boldsymbol{n}_y) q(\boldsymbol{x}) \, \mathrm{d}y - \int_{\Omega} G(\boldsymbol{x}, \boldsymbol{y}) q(\boldsymbol{x}) \, \mathrm{d}y. \tag{33}$$

Here, k is a constant between 0 and 1. If we do the Taylor's expansion of $g(\boldsymbol{x}, \boldsymbol{y}+k\epsilon\boldsymbol{n}_{\boldsymbol{y}})$ and $G(\boldsymbol{x}, \boldsymbol{y}+k\epsilon\boldsymbol{n}_{\boldsymbol{y}})$ about $(\boldsymbol{x}, \boldsymbol{y})$ with respect to ϵ, we obtain

$$g(\boldsymbol{x}, \boldsymbol{y} + k\epsilon\boldsymbol{n}_{\boldsymbol{y}}) = g(\boldsymbol{x}, \boldsymbol{y}) + k\epsilon\boldsymbol{n}_{\boldsymbol{y}} \cdot \boldsymbol{\nabla}_{\boldsymbol{y}} g(\boldsymbol{x}, \boldsymbol{y}) + \mathrm{O}(\epsilon^2), \tag{34}$$

$$G(\boldsymbol{x}, \boldsymbol{y} + k\epsilon\boldsymbol{n}_{\boldsymbol{y}}) = G(\boldsymbol{x}, \boldsymbol{y}) + k\epsilon\boldsymbol{n}_{\boldsymbol{y}} \cdot \boldsymbol{\nabla}_{\boldsymbol{y}} G(\boldsymbol{x}, \boldsymbol{y}) + \mathrm{O}(\epsilon^2). \tag{35}$$

Inserting these into the above two error equations, we obtain linear expressions in ϵ for the absolute errors when ϵ is sufficiently small.

$$L_{\mathrm{error}} = -\epsilon \int_{\partial\Omega} k\boldsymbol{n}_{\boldsymbol{y}} \cdot \boldsymbol{\nabla}_{\boldsymbol{y}} g(\boldsymbol{x}, \boldsymbol{y}) \, \mathrm{d}y + \mathrm{O}(\epsilon^2), \tag{36}$$

$$P_{\mathrm{error}} = -\epsilon \int_{\partial\Omega} k\boldsymbol{n}_{\boldsymbol{y}} \cdot \boldsymbol{\nabla}_{\boldsymbol{y}} G(\boldsymbol{x}, \boldsymbol{y}) \, \mathrm{d}y + \mathrm{O}(\epsilon^2). \tag{37}$$

The total error, T_{error} is

$$T_{\mathrm{error}} = L_{\mathrm{error}} + P_{\mathrm{error}}. \tag{38}$$

Thus, the total error is linear in ϵ also. This is consistent with perturbation theory for BVPs for linear PDEs when $\partial\Omega$ is smooth [13].

This slow convergence of WOS, i.e. the linearity of the error associated with the ϵ-shell in ϵ, supports the efficiency of GFFP versus WOS when accuracy beyond a preset limit is required [11]. The GFFP is an $\epsilon = 0$ method, and so where it can be used, this study shows that it should be used.

Acknowledgements

References

[1] M.E. Müller, Some continuous Monte Carlo methods for the Dirichlet problem, Ann. Math. Stat. 27 (1956) 569–589.

[2] A. Haji-Sheikh, E.M. Sparrow, The solution of heat conduction problems by probability methods, J. Heat Transfer 89 (1967) 121–131.

[3] H.-X. Zhou, A. Szabo, J.F. Douglas, J.B. Hubbard, A Brownian dynamics algorithm for caculating the hydrodynamic friction and the electrostatic capacitance of an arbitrarily shaped object, J. Chem. Phys. 100 (5) (1994) 3821–3826.

[4] J.A. Given, J.B. Hubbard, J.F. Douglas, A first-passage algorithm for the hydrodynamic friction and diffusion-limited reaction rate of macromolecules, J. Chem. Phys. 106 (9) (1997) 3721–3771.

[5] K.K. Sabelfeld, Monte Carlo Methods in Boundary Value Problems, Springer, Berlin, 1991.

[6] R. Ettelaie, Solutions of the linearized Poisson–Boltzmann equation through the use of random walk simulation method, J. Chem. Phys. 103 (9) (1995) 3657–3667.

[7] B.S. Elepov, G.A. Mihailov, The "Walk On Spheres" algorithm for the equation $\delta u - cu = -g$, Soviet Math. Dokl. 14 (1973) 1276–1280.

[8] T.E. Booth, Exact Monte Carlo solution of elliptic partial differential equations, J. Comput. Phys. 39 (1981) 396–404.

[9] T.E. Booth, Regional Monte Carlo solution of elliptic partial differential equations, J. Comput. Phys. 47 (1982) 281–290.

[10] J.A. Given, C.-O. Hwang, M. Mascagni, Continuous path Brownian trajectories for diffusion Monte Carlo via first- and last-passage distributions, Lect. Notes Comput. Sci. 2179 (2001) 46–57.

[11] C.-O. Hwang, J.A. Given, M. Mascagni, The simulation–tabulation method for classical diffusion Monte Carlo, J. Comput. Phys. 174 (2) (2001) 925–994.

[12] J.M. DeLaurentis, L.A. Romero, A Monte Carlo method for Poisson's equation, J. Comput. Phys. 90 (1990) 123–139.

[13] F. John, Partial Differential Equations, Springer, Berlin, Heidelberg, New York, 1982.

[14] J.D. Jackson, Classical Electrodynamics, Wiley, New York, 1975.

[15] H.-X. Zhou, Comparison of three Brownian-dynamics algorithms for calculating rate constants of diffusion-influenced reactions, J. Chem. Phys. 108 (19) (1998) 8139–8145.

[16] H.-X. Zhou, On the calculation of diffusive reaction rates using Brownian dynamics simulations, J. Chem. Phys. 92 (5) (1990) 3092–3095.

[17] S.D. Traytak, M. Tachiya, Diffusion-controlled reaction rate to asymmetric reactants under Coulomb interaction, J. Chem. Phys. 102 (23) (1995) 9240–9247.

[18] M. Freidlin, Functional Integration and Partial Differential Equations, Princeton University Press, Princeton, NJ, 1985.

[19] K.L. Chung, Z. Zhao, From Brownian Motion to Schrödinger's Equation, Springer, Berlin, 1995.

[20] S. Torquato, I.-C. Kim, D. Cule, Effective conductivity, dielectric constant, and diffusion coefficient of digitized composite media via first-passage-time equations, J. Appl. Phys. 85 (1999) 1560–1571.